Adaptive filtering for the Lattice Boltzmann Method.

S. Marié[a,c], X. Gloerfelt[b,c]

[a]*Conservatoire National des Arts et Métiers Email: simon.marie@lecnam.net*
[b]*Ecole Nationale Supérieure des Arts et Métiers*
[c]*Laboratoire DynFluid*

Abstract

In this study, a new selective filtering technique is proposed for the Lattice Boltzmann Method. This technique is based on an adaptive implementation of the selective filter coefficient σ. The proposed model makes the latter coefficient dependent on the shear stress in order to restrict the use of the spatial filtering technique in sheared stress region where numerical instabilities may occur. Different parameters are tested on 2D test-cases sensitive to numerical stability and on a 3D decaying Taylor Green vortex. The results are compared to the classical static filtering technique and to the use of a standard subgrid-scale model and gives significant improvements in particular for low-order filter consistent with the LBM stencil.

Keywords: Lattice Boltzmann Method, Adaptive filtering, Numerical stability, Taylor-Green vortex

Introduction

The Lattice Boltzmann Method [1][2] (LBM) is nowadays recognized as a fast and reliable method to simulate the dynamics of weakly compressible flows. Some studies [3, 4, 5, 6] have shown the capabilities of LBM to perform complex and multi-physical simulations from turbulent flows to aeroacoustic applications thanks to the low dissipation error introduced by the method. As a counterpart, LBM suffers from numerical instabilities when Reynolds number becomes high.

The origins of LBM instabilities have been actively studied and remains an open subject [7, 8, 9, 10]. The main consequence of the inherent LBM instability is to create diverging oscillations mainly characterized by high frequencies which propagate in the whole domain. These numerical instability waves are often generated by unadapted initial conditions, geometric singularities or in region where high gradients are observed. In industrial applications, several of these numerical constraints are present, thus computations often become dramatically unstable.

Numerous studies have proposed stabilization techniques based on different approaches such as multiple relaxation times [11], regularization techniques [12], energy conserving [13], entropic models or positivity enforcing [14]. The vast majority of these models consists in a theoretical modification of the LBM scheme and gives relevant informations about the unstable nature of LBM. As a counterpart, lots of stabilizing strategies have a global effect on the viscosity thus modifying the effective Reynolds number or increasing the global dissipation of the method. This dissipation inherent to the construction of more stable schemes can impact the evaluation of pressure fluctuations whose accuracy is crucial (e.g. for aeroacoustic simulations). In that case a local strategy would be preferred in order to distinguish spatial zones where a stabilization is required to those in which the standard LBM scheme can be applied.

Ricot et al.[15] proposed to use selective spatial filters[16] to stabilize the method by increasing the dissipation in the high wavenumber range where the LBM instabilities occur, keeping a low dissipation at small wavenumbers. This approach can be applied to aeroacoustic simulations by maintaining an acceptable level of dissipation error at

low wavenumbers. However, this method basically applies to the whole domain and becomes unavailing outside of sheared regions where numerical instabilities have less chances to develop. Furthermore, the use of high-order filters increases the stencil of LBM which is low by nature and leads to a loss of locality of the method which is penalizing for massively parallel computations. Finally, from a dynamical point of view, the selective spatial filters have never been tested on transition situation where the time evolution prediction is of major importance for the accuracy of the results. Therefore, the need for a local and adaptive stabilization procedure is relevant and should be carried out, in particular in the framework of the Lattice Boltzmann Method.

The idea of the present study is to propose an improved filtering strategy restricted to highly sheared regions [9] keeping weakly sheared ones free of artificial dissipation. The choice of the shear stress as a segregation parameter is highly motivated by the large eddy simulation framework where the shear stress sensitivity is of crucial importance in the construction of subgrid-scale models [17, 18]. Moreover, this study can be included in the framework of other local approaches where additional numerical treatment is done in restricted zones of interest [19, 20, 21]. Therefore the present study aims at introducing a shear-stress selectivity in the application of spatial filtering. The proposed strategy is developed in the framework of the Lattice Boltzmann Method and applied to unsteady test-cases highly sensitive to numerical dissipation.

After a brief presentation of the Lattice Boltzmann model in section 2, the new filtering strategy is described in section 3 and validated in sections 4, 5 and 6 on 2D and 3D test-cases with some comparisons to the traditional filtering techniques. Finally, section 7 is dedicated to computational cost issues.

Lattice Boltzmann Method

The Lattice Boltzmann method[1] is described by the following algorithm:

$$g_\alpha(\mathbf{x} + \mathbf{c}_\alpha \Delta \mathbf{t}, t + \Delta t) = g_\alpha(\mathbf{x}, t) - \frac{1}{\tau_g}[g_\alpha(\mathbf{x}, t) - g_\alpha^{eq}(\mathbf{x}, t)] \tag{1}$$

where g_α are distribution functions computed on a regular velocity lattice $\mathbf{c}_\alpha$, colliding and relaxing to a local equilibrium g_α^{eq} with a relaxing parameter $\tau_g = \dfrac{\nu}{\tilde{c}_0^2} + \dfrac{1}{2}$ where ν and $\tilde{c}_0$ are the nondimensional viscosity and speed of sound respectively. In this study, we use the $D2Q9$ and $D3Q19$ models for $2D$ and $3D$ simulations. The classical parameters of the model are defined as follows:

$$g_\alpha^{eq}(\mathbf{x}, t) = \rho \omega_\alpha (1 + \frac{\mathbf{u}.\mathbf{c}_\alpha}{\tilde{c}_0^2} + \frac{(\mathbf{u}.\mathbf{c}_\alpha)^2}{2\tilde{c}_0^4} - \frac{|\mathbf{u}|^2}{2\tilde{c}_0^2}) \tag{2}$$

$$\omega_\alpha = \begin{cases} D2Q9 & \dfrac{4}{9}, \dfrac{1}{9}, \dfrac{1}{36} \quad , \quad \alpha = 0, \alpha = 1..4, \alpha = 5..8 \\[2ex] D3Q19 & \dfrac{1}{3}, \dfrac{1}{18}, \dfrac{1}{36} \quad , \quad \alpha = 0, \alpha = 1..6, \alpha = 7..18 \end{cases} \qquad \tilde{c}_0^2 = \frac{1}{3} \tag{3}$$

$$\Delta t = \frac{\tilde{c}_0 \Delta x}{c_0} \tag{4}$$

The macroscopic quantities ρ and $\mathbf{u}$ can be computed from the distribution functions with the discrete moments:

$$\rho = \sum_\alpha f_\alpha \tag{5}$$

$$\rho \mathbf{u} = \sum_\alpha \mathbf{c}_\alpha f_\alpha \tag{6}$$

The pressure is recovered by the relation:

$$p = \tilde{c}_0^2 \rho \tag{7}$$

Based on these parameters, it can be shown [2] that LBM simulates the compressible Navier-Stokes equations in the limit of low Mach numbers with a second-order accuracy in space and time.

Adaptive selective spatial filters

As proposed by Ricot et al [15], the stability of LBM can be enhanced by space-filtering the moments of eq.(5) and (6). Spatial filtering of a quantity Q is defined by subtracting a weighted combination of the symmetric neighboring points in each direction:

$$\langle Q(\mathbf{x}) \rangle = Q(\mathbf{x}) - \sigma \sum_{j=1}^{D} \sum_{n=-N}^{N} d_n Q(\mathbf{x} + n\Delta x_j) \tag{8}$$

where σ is a coefficient between 0 and 1, often taken to 0.1, d_n are coefficients depending on the filter order and D is the number of spatial dimensions. In this study, classical 3-point, 5-point stencil and optimized 9-point stencil filters are used [16]. The coefficients of the filters are given in table 1.

	d_0	d_1	d_2	d_3	d_4
3-point	1/2	−1/4			
5-point	6/16	−4/16	1/16		
9-point (optimized [16])	0.243527493120	−0.204788880640	0.120007591680	−0.045211119360	0.008228661760

Table 1: Coefficients of the selective filters: $d_n = d_{-n}$.

Different filtered quantity can be chosen according to the LBM scheme with the following possibilities with increasing computational cost:

1. Filtering moments: $\rho, \mathbf{u}$ ($D + 1$ tables).
2. Filtering distribution functions: g_α (N_v tables).
3. Filtering collision operator: $-\dfrac{1}{\tau_g}(g_\alpha - g_\alpha^{eq})$ (N_v tables).

where D is the number of physical dimensions and N_v is the number of discrete velocities. In order to limit computational cost, the first solution will be preferred in this study and the influence of the filtered quantity will be discussed in section 6.

In the wavenumber space, Ricot et al. [15] have shown by a linear stability analysis that the explicit filtering introduce an additional dissipation linked to the coefficient:

$$\kappa(\mathbf{k}) = 1 - \sigma\mathcal{F}(\mathbf{k}) \tag{9}$$

where $\mathcal{F}(\mathbf{k})$ is the transfer function of the explicit filter as a function of the wavenumber vector $\mathbf{k}$. Then the global efficiency of such a filter is led by both $\mathcal{F}(\mathbf{k})$ and σ. The idea of this study is to make the coefficient σ of relation (8) dependent on the shear stress. For instance, let us consider $\sigma_d(\mathbf{x})$ to be of the form:

$$\sigma_d(\mathbf{x}) = \sigma_0 \left(1 - e^{-(|S(\mathbf{x})|/S_0)^2}\right)^2 \tag{10}$$

where $|S| = \sqrt{2S_{ij}S_{ij}}$ and σ_0 is the static filter amplitude. S_0 is a reference shear stress amount defining a sensitivity from which the dynamical filter starts to be active. The quantity $|S|$ is evaluated in the Lattice Boltzmann framework, from the second order moment:

$$\tau_{ij} = 2\rho\nu S_{ij} = -\sum_\alpha c_{\alpha,i} c_{\alpha,j} (g_\alpha - g_\alpha^{eq}) \tag{11}$$

which gives:

$$|S| = \frac{\mathbf{Q_f}}{2\rho\nu} \tag{12}$$

with $\mathbf{Q_f} = \sqrt{2P_{ij}P_{ij}}$ and $P_{ij} = \sum_\alpha c_{\alpha,i}c_{\alpha,j}(g_\alpha - g_\alpha^{eq})$. Relation (12) is often used for the implementation of subgrid-scale models in the Lattice Boltzmann Method [22, 23] and does not require any derivative computations.

Thenceforth, a crucial point relies in the estimation of the sensitivity shear stress S_0. When the shear stress is low ($|S| < S_0$), the filter has no effect ($\sigma_d \sim 0$) and when the shear stress rises to higher values ($|S| > S_0$), the filter acts normally ($\sigma_d \sim \sigma_0$). Then S_0 can be seen as a shear sensitivity parameter and is of major importance in the dynamical filtering efficiency. If S_0 is chosen smaller than the minimum amount of shear stress (S_{min}), the filter coefficient σ_d will be close to σ_0 in the whole domain and the adaptive filter will behave like a classical static filter. Conversely, if S_0 is chosen higher than the maximum amount of shear stress (S_{max}), σ_d will be very low in the whole domain and the adaptive filter will have almost no effect. Consequently, the present methodology becomes efficient for intermediate values of S_0: $S_{min} < S_0 < S_{max}$. Its influence is sketched up in figure 1.
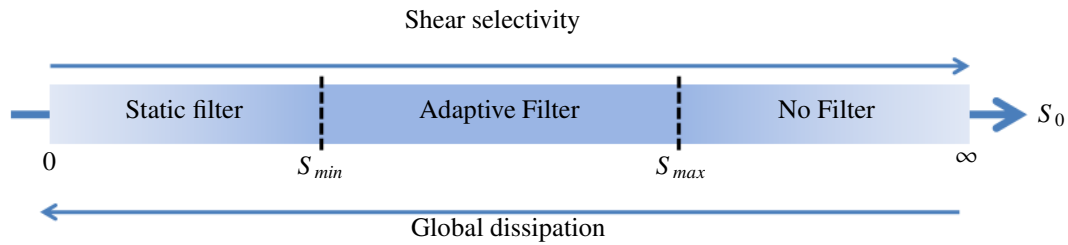

Figure 1: Shear stress sensitivity

In this study S_0 is evaluated in terms of the maximum amount of shear stress: $S_0 = \xi S_{max}$ where ξ is a selectivity parameter close to unity and S_{max} can be evaluated by two different ways:

1. Computed value: evaluation of $max(|S|)$ at each timestep based on instantaneous or mean field.
2. Imposed value: Imposed constant value at initialization based on physical, numerical or empirical criteria.

The first type of estimation has a straightforward implementation and implies that the maximum value of σ_d remains close to a constant in time: $\sigma_d = \sigma_0 \left(1 - e^{-(1/\xi^2)}\right)^2$ and could be used if the aim is to control the overall dissipation induced by the filter.

The second type of estimation imposes a fixed amount of shear stress from which the filter will be active. In that case, the time evolution of the effective stress would lead to a time evolution of the filter coefficient σ_d. A first basic criterion for the estimation of S_{max} can be based on the ratio between a velocity scale U and a length scale δ:

$$S_{max} = \frac{U}{\delta} \tag{13}$$

Equation (13) is evaluated at initialization step based on the prescribed simulation parameters.

Another way to evaluate S_{max} can be based on a numerical criterion assessing the positivity of the distribution function g_α as a numerical stability criterion [24]. Indeed, assuming that the quantities g_α must be positive, an upper limit can be found for relation (12) by substituting g_α with zero and considering the second-order moment:

$$\sum_\alpha c_{\alpha,i}c_{\alpha,j}g_\alpha^{eq} = \rho u_i u_j \tag{14}$$

which yields:

$$|S| = \frac{\mathbf{Q_f}}{2\rho\nu} = \frac{\sqrt{2 \sum_\alpha c_{\alpha,i}c_{\alpha,j}g_\alpha^{eq} \sum_\alpha c_{\alpha,i}c_{\alpha,j}g_\alpha^{eq}}}{2\rho\nu} \leq \frac{\sqrt{2}u_i u_j}{2\nu} \tag{15}$$

Then S_{max} ensuring the stability condition can be written from (15) by only keeping the leading term of the linearized $u_i u_j$:

$$S_{max} = \frac{\sqrt{2}U_0^2}{2\nu} \sim \frac{Re_\delta U_0}{\delta} \tag{16}$$

where δ is the characteristic length scale. It should be noticed that, by construction, relation (16) is given in lattice units and implicitly contains the mesh size information. Indeed, in dimensional units, relation (16) would be multiplied by $1/\Delta t$ which depends on Δx (see relation (4)). Thus for coarse grids, relation (16) will give smaller value of S_{max} than for fine grids, which is consistent with stability issues.

In the following, the proposed adaptive filtering procedure is studied on illustrative test cases with different evaluations of S_{max} following the nomenclature presented in table 2.

Simulation name	F_s	F_{ad}^0	F_{ad}^1	F_{ad}^2
type	Static	Adaptive	Adaptive	Adaptive
S_0	0	$\xi max(|\mathbf{S}|)$	ξS_{max}	ξS_{max}
S_{max}	×	Computed	Imposed by (13)	Imposed by (16)

Table 2: Reference names used for the simulations

First, a convected 2D vortex is used to characterize the influence of the present filtering strategy on the local dissipation, then the flow past a square cylinder is investigated to demonstrate the stabilizing capabilities of the adaptive filtering and finally, the simulation of a 3D decaying Taylor-Green vortex is performed to demonstrate the effectiveness of the present filtering on a fully 3D turbulent flow.

Application to a 2D convected vortex

Test case implementation

The 2D convected vortex is a simple test case which is used here to characterize the effects of the adaptive filter on the dissipation of a simple coherent structure. For this configuration, the amount of shear stress is maximum near the vortex boundary where the filter is expected to be active, leaving the vortex centre free of artificial dissipation.

In the purpose of characterizing the amount of numerical dissipation induced by the present methodology, the computations are performed for an inviscid vortex by setting the relaxation time to 0.5 (e.g. $\nu = 0$). The Mach number is set to $M_\infty = 0.1$ and the initial field is defined as follows :

$$
\begin{cases}
\rho &= 1 \\
u &= U_\infty + \varepsilon U_\infty (y - y_0) \exp\left[-\frac{\ln(2)}{b_p^2}\left((x - x_0)^2 + (y - y_0)^2\right)\right] \\
v &= -\varepsilon U_\infty (x - x_0) \exp\left[-\frac{ln(2)}{b_p^2}\left((x - x_0)^2 + (y - y_0)^2\right)\right]
\end{cases}
\tag{17}
$$

with $(x_0, y_0) = (n_x/2, n_y/2)$, $\varepsilon = 10^{-3}$ and $b_p = 20$. The grid (n_x, n_y) is set to 256×128 points with periodic boundary conditions and the number of time-steps is chosen so as to achieve at least ten vortex crossings of the domain.

Results and discussions

For this test case, only the low-order 3-point filter is considered and the static filter coefficient is set to $\sigma_0 = 0.1$. Different estimations of S_0 are tested summarized in table 2. The F_{ad}^0 estimation is based on the computation of $S_{max} = max(|\mathbf{S}|)$ at each timestep, F_{ad}^1 imposes a value of S_{max} based on (13) with $U = \varepsilon U_0$ and $\delta = b_p$ and F_{ad}^2 imposes S_{max} from (16).

(a)   (b)
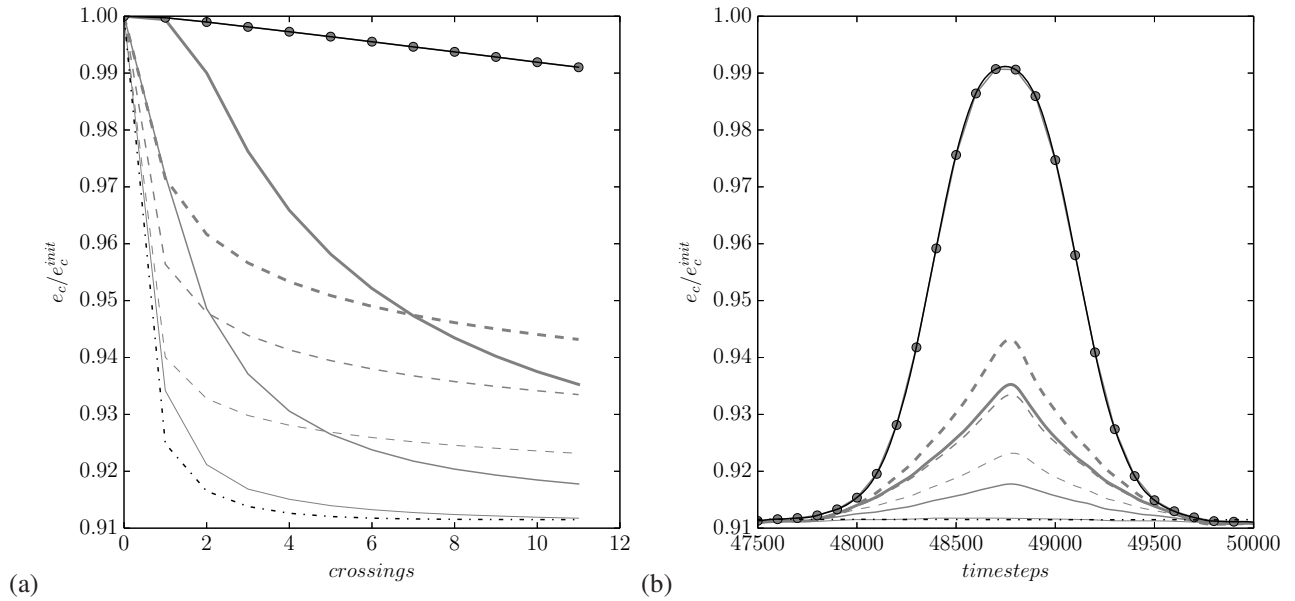
Figure 2: (a) Evolution of the maximal amplitude of the vortex kinetic energy at each crossing of the domain. (b) Time trace of the normalized kinetic energy at the centre point location after the last crossing of the domain. (—): Without filtering, (-·-): F_s, (—): F_{ad}^0, (- -): F_{ad}^1, (-•-): F_{ad}^2. Thin lines to thick lines are for $\xi = 0.5$, $\xi = 1.0$ and $\xi = 1.5$.

Figure 2 shows the time evolution of the kinetic energy computed at the centre point of the domain for various values of ξ. The classical filtering procedure with a constant coefficient $\sigma = 0.1$ is also added for comparison.

When the filter acts with the same amount in the whole domain (classical filter) the introduced dissipation has damped the major part of the initial kinetic energy confirming that the classical low-order filter is too dissipative when applied in the whole domain. Figure 3 represents the isocontours of σ_d at a given timestep for different estimations of S_0 and different values of ξ. As expected, non-zero values of σ_d are concentrated near the vortex boundary and reach null values in the vortex centre. The results indicate less dissipation from the F_{ad}^2 estimation based on relation (16) because the imposed value of S_{max} is never reached and σ_d remains small all along the vortex convection for all considered values of ξ. Indeed, the convected vortex is numerically stable and instability waves are not observed for
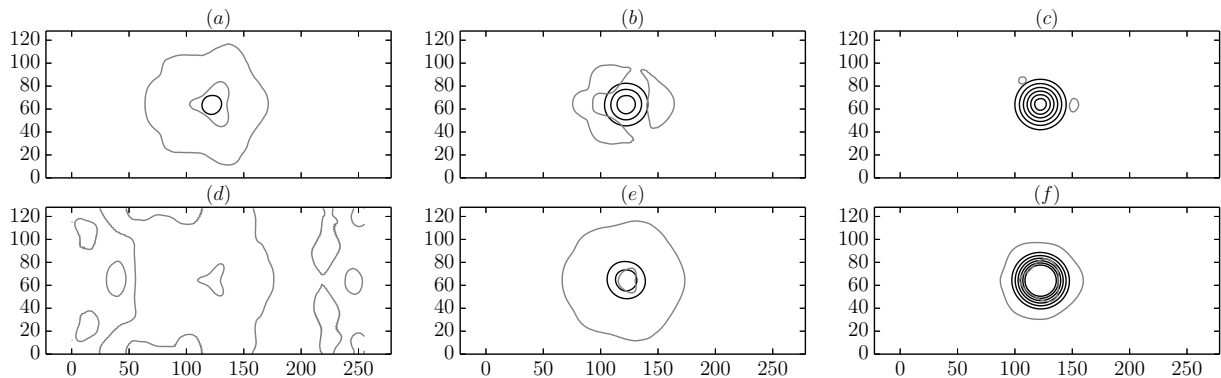

Figure 3: (—) Isocontours of density and (—) isocontours of $\sigma_d = 0.1\sigma_0$ after 13200 timesteps. (a-c) F_{ad}^1 with $\xi = 0.5, 1.0$ and 1.5. (d-f) F_{ad}^0 with $\xi = 0.5, 1.0$ and 1.5.

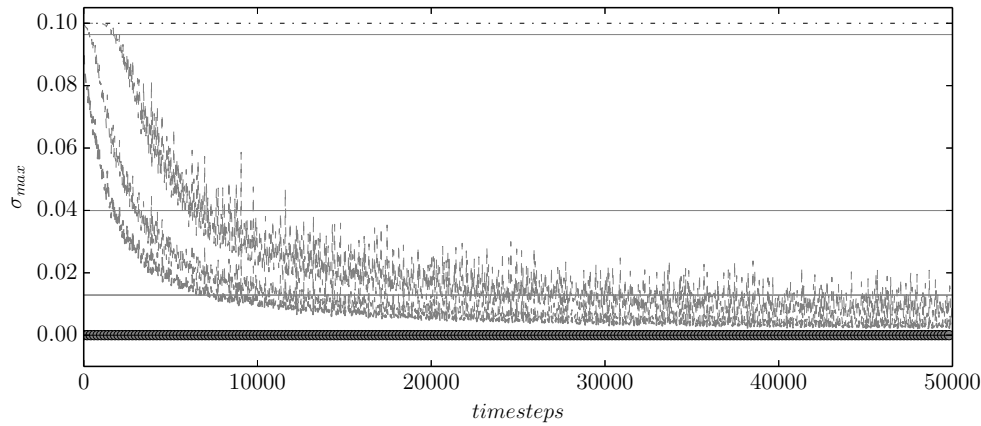this test case which implies that the filter is almost never active.

Figure 4: Time trace of the maximum value of the coefficient σ_d. (—): Without filtering, (⋯): F_s, (—): F_{ad}^0, (- -): F_{ad}^1, (-•-): F_{ad}^2. Thin lines to thick lines are for $\xi = 0.5$, $\xi = 1.0$ and $\xi = 1.5$.

For low values of ξ the shear selectivity of the adaptive filter is weak and the behaviour is close to the one obtained with the classical filters. The F_{ad}^1 estimation induces high values of σ_d at initialization due to the similarity between the imposed S_{max} and the local shear stress. When the vortex is convected, its energy is dissipated by the filter inducing a decrease of the shear stress then leading to a reduction of the filter coefficient as depicted in figure 4. Then the filter impact becomes weaker when the local stress is lower than the imposed threshold value. On the other hand, the F_{ad}^0 estimation induces high level of dissipation because the threshold value S_{max} is computed from the local shear stress and gives higher value of σ_d when the shear stress is low. The filter effect in this case remains constant in time, as illustrated in figure 4 and gives highly dissipated results after ten crossings of the domain.

These observations show that the numerical dissipation introduced by the filter can be controlled by the shear stress selectivity. The F_{ad}^0 and F_{ad}^1 estimations lead to dissipated results because of the under-estimation of S_{max} whereas the F_{ad}^2 estimation shows a good ability to switch off the filter if instability waves are not detected. Then in the following, only the F_{ad}^2 estimation will be retained and will now be studied in the context of numerical stability issues.

Application to the flow past a square cylinder

Test case implementation

In this section we are considering the flow past a 2D square cylinder which is known to exhibits some strong numerical instabilities for Reynolds numbers larger than 500. The computations are performed on a uniform 500×200 points grid with a 10×10 points solid square located at $(x_s, ys) = (100, 100)$. Wall boundary conditions are implemented with the classical bounce-back method to ensure a null velocity at the wall, and periodic boundary conditions are used at the domain boundary with a sponge zone at the outlet in order to damp outgoing structures. The sponge zone has a Gaussian shape and is defined by:

$$\frac{\nu}{\nu_0} = \alpha \exp\left[-\frac{\ln(2)}{m^2}(x - p)^2\right] \tag{18}$$

For this study, the parameters have been fixed to, $\alpha = 200$, $m = 50$ and $p = n_x - 75$ meaning that the viscosity start to increase from ν_0 to $200\nu_0$ in the last 100 grid points of the domain. The Reynolds based on the square side is $Re_D = 800$ and the Mach number is set to $M_\infty = 0.25$. For these parameters, the classical LBM-BGK method becomes highly unstable and leads to collapsing computations. Consequently some artificial dissipation must be added to damp instability waves.

Here, the present filtering strategy is tested and compared to the classical static filter for the 3-point stencil filter. In this study, the quantities at the wall are not filtered but the 3-point filter allows the close-neighboring points of the wall quantities to be filtered normally. However, as discussed in [21], the use of explicit filtering near the wall is conditioned by a relatively high wall-resolution. For the present test-case, the wall resolution is set intentionally coarse in order to exhibit numerical instability. Then the present adaptive technique is expected to modify the near-wall quantities where a high shear stress is detected yielding a high value for the filter coefficient.

For this test-case, the σ_0 parameter is set to 0.1 and the F_{ad}^2 estimation is used for different values of ξ and compared to the classical static filter.

Results and discussions

The isocontours of vorticity displayed in figure 5 show that the classical low-order filter is too dissipative and leads to a laminar flow without vortex shedding. This confirms that these kind of low-order filter should not be applied for unsteady simulations. In contrast, the present adaptive filtering technique exhibits unsteady flow with identified vortex shedding in the cylinder wake. All the value of ξ give similar wakes with a slight delay in the establishment of the vortex shedding for the lowest value of ξ due to a too high dissipation close to the wall. These observations are confirmed by looking at the drag and lift coefficient of table 3 which are slightly underestimated as ξ is decreased due to the use of near-wall filtering with low resolution.

	C_d^{mean}	C_l^{rms}
$\xi = 0.5$	0.825	0.08
$\xi = 1.0$	0.831	0.09
$\xi = 1.5$	0.837	0.10

Table 3: Comparison of the average drag coefficient C_d^{mean} and rms lift coefficient C_l^{rms} for different values of *xi*.
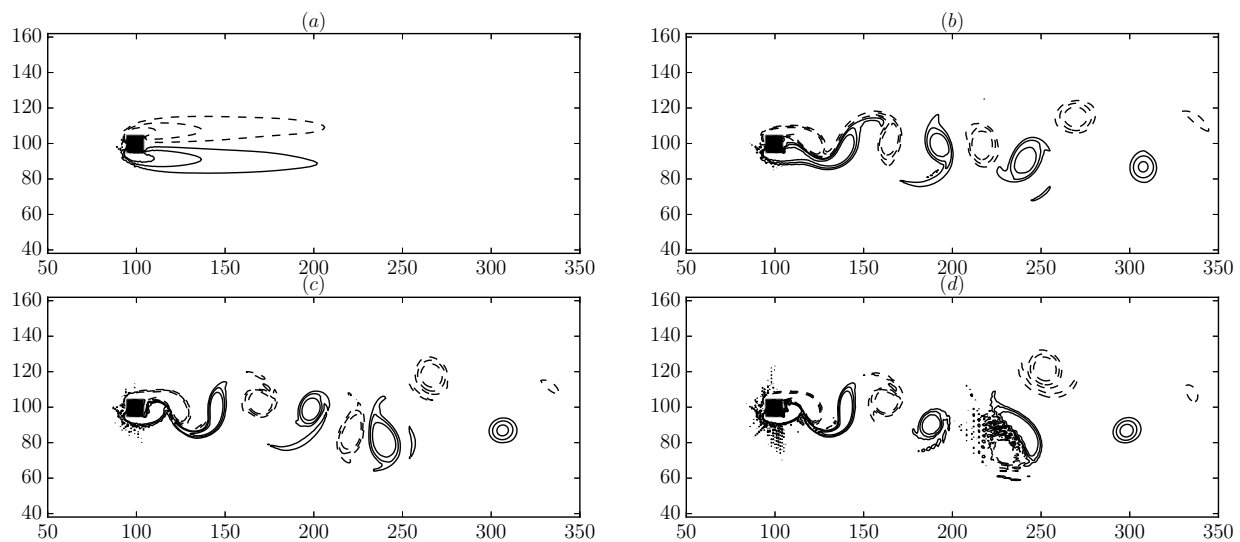

Figure 5: Isocontours of vorticity from -0.02 to 0.02 in lattice unit at time= 2000 timesteps. Dashed contours denotes negative values. (a) 3-point classic filter, (b) 3-point adaptive filter with $\xi = 0.5$, (c) $\xi = 1.0$ (d) $\xi = 1.5$.

By plotting the time evolution of σ_d at a wall point and a wake point in figure 6, we can see that the highest values of σ_d are reached near the wall where the shear stress is maximum. For the low value of ξ, σ_d is fluctuating around 60% of σ_0 near the wall whereas for the high value of ξ, σ_d is fluctuating around 1% of σ_0. From the signal

of the wake point, it could be inferred that σ_d remains smaller than 1% of σ_0 for both value of ξ except for $\xi = 1.5$ after 2000 timesteps. For this value of ξ, the simulation is close to the stability limit and oscillations are visible for high values of the shear stress. This phenomenon is observed in the vicinity of contra-rotative vortices which are getting very close to each other. An instability wave is created but the filter coefficient is not high enough to damp this instability. However, when the instability is developing, higher shear stress is detected and the filter coefficient is increased to 80% of σ_0 in few timesteps. Then the instability wave is damped and the filter coefficient decreases to very low values.
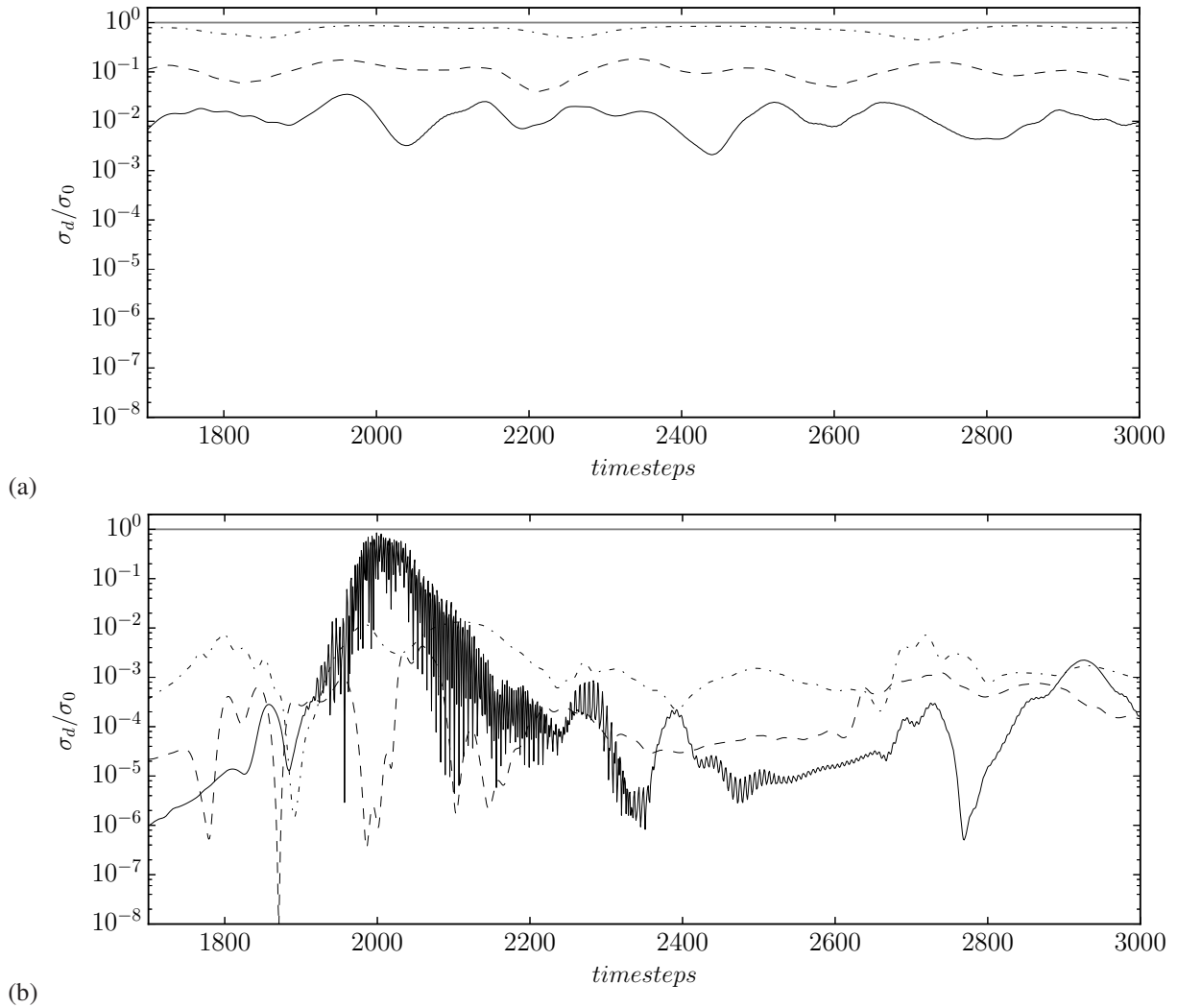

Figure 6: Time trace of filter coefficient σ_d at (a)$(x_c, y_c) = (100, 105)$ and (b)$(x_c, y_c) = (230, 85)$. (—: F_s), (−·− F_{ad}^2: $\xi = 0.5$), (- -: $\xi = 1.0$) and (—: $\xi = 1.5$).

These observations confirm the adaptive nature of the presented filtering strategy and show that low-order filters can be applied to unsteady flows if they are restricted to localized zones based on a shear criterion. Moreover, the estimation of S_{max} used for this test case gives relevant results in terms of stability control and demonstrates the ability of the adaptive filters to be an efficient stabilization procedure for the Lattice Boltzmann method.

Application to a 3D Taylor Green Vortex

Test case implementation

In order to study the effect of the present filtering technique on a 3D turbulent configuration, the decaying Taylor-Green vortex (TGV) is used. It is a fundamental test case used as prototype for vortex stretching and production of small-scale eddies and therefore allows the study of the dynamics of transition to turbulence. This test-case has been widely used to study the dissipation errors of numerical schemes [25]. In particular, Aubard et al. [26] have recently used this test-case to confront the selective filtering techniques to the use of subgrid-scale models.

The initialization of the Taylor-Green vortex is done by setting velocity and pressure variables as follows:

$$\begin{cases} p & = & p_\infty + \dfrac{\rho_\infty U_\infty^2}{16}[\cos(2z) + 2][\cos(2x) + \cos(2y)] \\ u & = & U_\infty \sin(x)\cos(y)\cos(z) \\ v & = & -U_\infty \cos(x)\sin(y)\cos(z) \\ w & = & 0 \end{cases} \tag{19}$$

In order to reduce numerical oscillations at the beginning of the simulation, the distribution functions g_α are initialized to their equilibrium state with an additional non-equilibrium part based on the Chapman-Enskog micro-scale expansion [27].

For this study, the simulations are performed on a 2π-periodic cubic domain with a Reynolds number of $Re = 1600$ based on a physical characteristic length of $L_{ref} = 1$m:

$$Re = \frac{U_\infty L_{ref}}{\nu_\infty} = \frac{\tilde{U}_\infty L_{ref}}{\Delta x \tilde{\nu}_\infty} \tag{20}$$

where $\tilde{\,}$ quantities denotes lattice unit quantities.

The Mach number is taken to $M_\infty = 0.085$ and $\rho_\infty = 1$ fixing the other parameters to $\tilde{U}_\infty = 0.049$ and $\tilde{p}_\infty = 1/3$ in lattice unit. The relaxation parameter is set with the Reynolds number to $\tau_g = \dfrac{\tilde{U}_\infty L_{ref}}{\Delta x \tilde{c}_0^2 Re} + \dfrac{1}{2}$.

The filter coefficient is here computed with F_{ad}^2 estimation of S_{max} based on relation (16) and different values of ξ are tested. Different filter types are also compared to analyze the influence of the filtering order on the flow dynamics. For the validation of this test case, the spectral data from Brachet et al. [28] are used and compared to our reference simulation on a 256^3 grid.

Results and discussion

A reference simulation is performed on a 256^3 grid without any filtering technique. Figure 7 displays the evolution of Q-criterion in the domain. The classical behavior of the Taylor-Green vortex is observed, the initial field gives rise to large vortices which are then stretched and lead to the production of small-scale eddies and decaying turbulence.

In the following, a series of tests are performed to characterize the present filtering strategy. First, the influence of the grid resolution on the non-filtered scheme is presented, then the influence of parameters σ_0 and S_0 in equation (10) are scrutinized and finally, comparisons with static filtering strategy and subgrid-scale model are performed.

Grid sensitivity

The lattice Boltzmann method is a second-order accuracy scheme in space and time. In the literature, few studies have been published on the validation of the 3D Taylor-Green vortex with LBM simulations [29]. It is thus interesting to see the capabilities of the standard *LBGK* scheme to simulate the dynamics of a 3D decaying vortex. For that purpose, the evolution of the kinetic energy dissipation rate $\epsilon = -\partial_t k$ is scrutinized for various resolutions from 64^3 to 256^3 and compared with the spectral simulation of Brachet et al. [28] in figure 8. In the following, the time is normalized
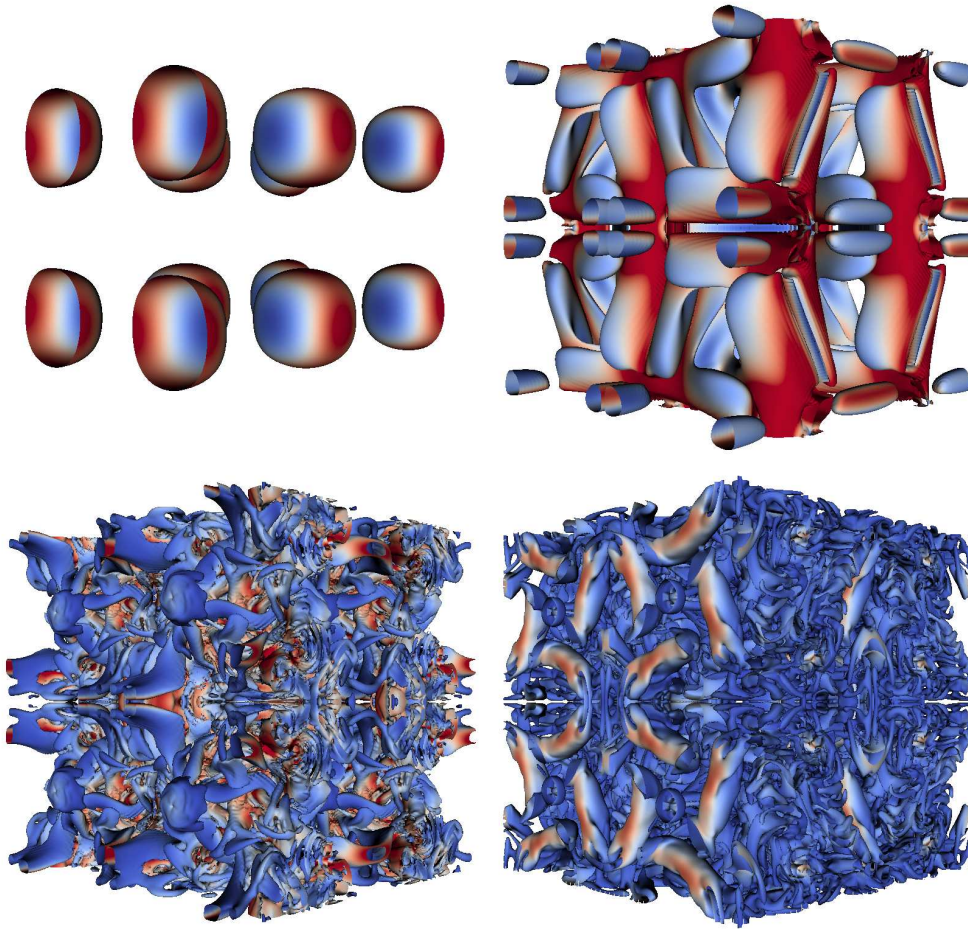
Figure 7: Isosurface of the Q-criterion colored by kinetic energy at time $t = 0, t = 4, t = 10, t = 16$ for $Re = 1600$ on a 256^3 grid.

with respect to the quantity L_{ref}/U_∞. The dissipation rate is computed with a second-order centered finite-difference approximation.

The TGV dynamical evolution is characterized by three main steps visible in the time trace of ϵ. First, the initial laminar state is transitioning to turbulence until the stretched vortex tubes break down into small scales around $t = 5$. Then the dissipation rate is rising to a sharp peak near $t = 9$ corresponding to the fully turbulent state which is then decaying similarly to an isotropic and homogeneous turbulence.

The results of the classical LBM simulations without any filtering technique are displayed in figure 8. The reference simulation on a 256^3 grid is seen to be in very good agreement with the spectral results. The 128^3 grid gives satisfactory results for the transition region but the peak in the dissipation rate is not properly captured and the decaying phase starts too early. The 64^3 and 96^3 simulations give rise to numerical instability at different time. The 96^3 grid simulation exhibits a relatively good transition to turbulence but collapses just before the peak of dissipation is reached around $t = 8$. Finally, the 64^3 grid simulation collapses earlier around $t = 5$, when the stretched vortex tubes break down into small scales.

Thus, the LBM scheme shows a good ability to simulate the Taylor-Green vortex dynamics when using fine grids but is limited by its inherent instability for coarser grids and high Reynolds numbers. Therefore the use of a stabilizing strategy becomes a crucial point to investigate turbulent simulations with the Lattice Boltzmann Method.
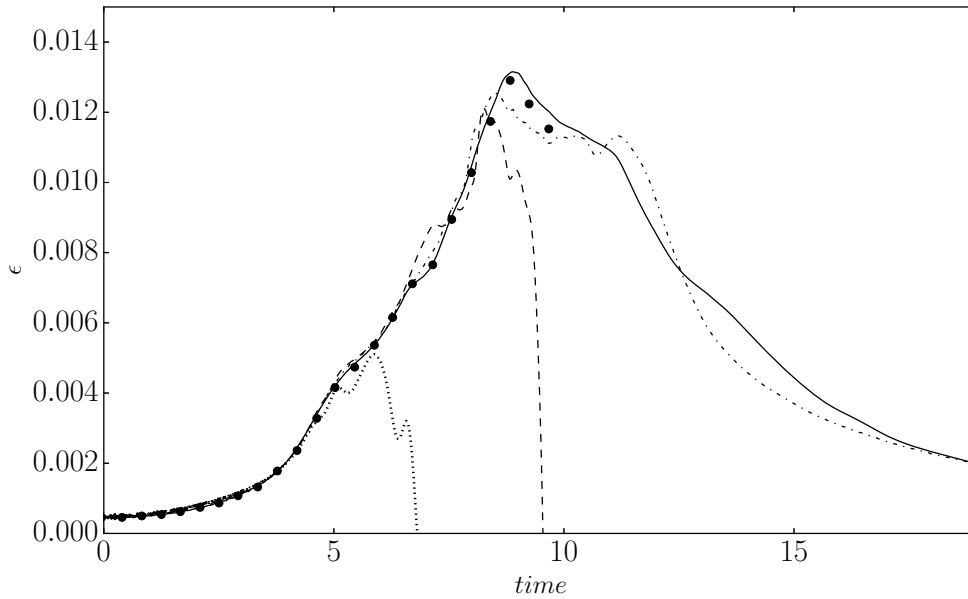
Figure 8: Non dimensional time evolution of the dissipation rate ϵ. ($\bullet$ spectral data), (... 64^3), (- - 96^3), ($- \cdot - 128^3$) and (—— 256^3)

Influence of σ_0 and ξ

As described in section 3, the dynamical filtering strategy is sensitive to two main parameters which are σ_0 and ξ. The first one determines the filtering amplitude when the shear stress is high and could be seen as the efficiency of the filter. The latter one plays the role of shear stress selectivity and is essential for controlling the dissipation amount of the filtering technique as described in the previous sections. The sensitivity to these parameters is investigated on a 96^3 grid for various values of σ_0, ξ and the different selective filters presented in table 1.

A first sensitivity analysis is performed on the σ_0 parameter with a fixed value of $\xi = 1$. Results are reported in figure 9-left and exhibit relatively similar behaviour. A high value of σ_0 induces more damped results, in particular after the vortex breakdown near $t = 5$ when the filter order is low. On the other hand, better results are obtained for low σ_0 values. This improvement is particularly visible for the 3-point filter which can fairly reproduce the vortex breakdown around $t = 5$ when σ_0 is set to 0.01. Lower values of σ_0 have been tested but lead to unstable simulations. This suggest that the dynamical filtering strategy should be applied for values of σ_0 as low as possible in the limit of stability. By looking at figure 9-right where the time evolution of σ_d is represented, one can see that the value of σ_0 has a direct impact on the time evolution of σ_d. Indeed, when σ_0 changes, the filtering amount is modified and so is the shear stress which modifies the local σ_d value. Moreover, for higher values of σ_0 the maximum value of σ_d is never reached suggesting that the filtering amount induces lower shear stress and in turn reduces σ_d. On the other hand, when σ_0 is low, the filtering amount allows larger shear stress values then increasing σ_d close to its maximum value fixed by σ_0. However, these considerations depend also on the shear stress selectivity which is driven by the value of S_0.

The second sensitivity analysis is performed on the parameter ξ which controls S_0 and for a fixed value of $\sigma_0 = 0.05$. Results are reported in figure 10-left which shows that the selected ξ values have an important impact on the results. A lower sensitivity induces an earlier filtering activity which damps the initial laminar state and lead to a wrong dissipation rate evolution. Indeed, results of figure 10-right indicate that σ_d starts to increase from a non zero value for low sensitivity parameters. In contrast, when the sensitivity is high, the filter does not act in low sheared region and is activated only when large vortices have broken up and small-scales structures are developing to turbulence. Moreover it could be seen from figure 10 that the effect of the filter order is reduced when increasing the sensitivity. Indeed, 3-point filter results are close to those of the 9-point filter when sensitivity is high. This is an important outcome in terms of computational cost suggesting that the filter order could be reduced when increasing
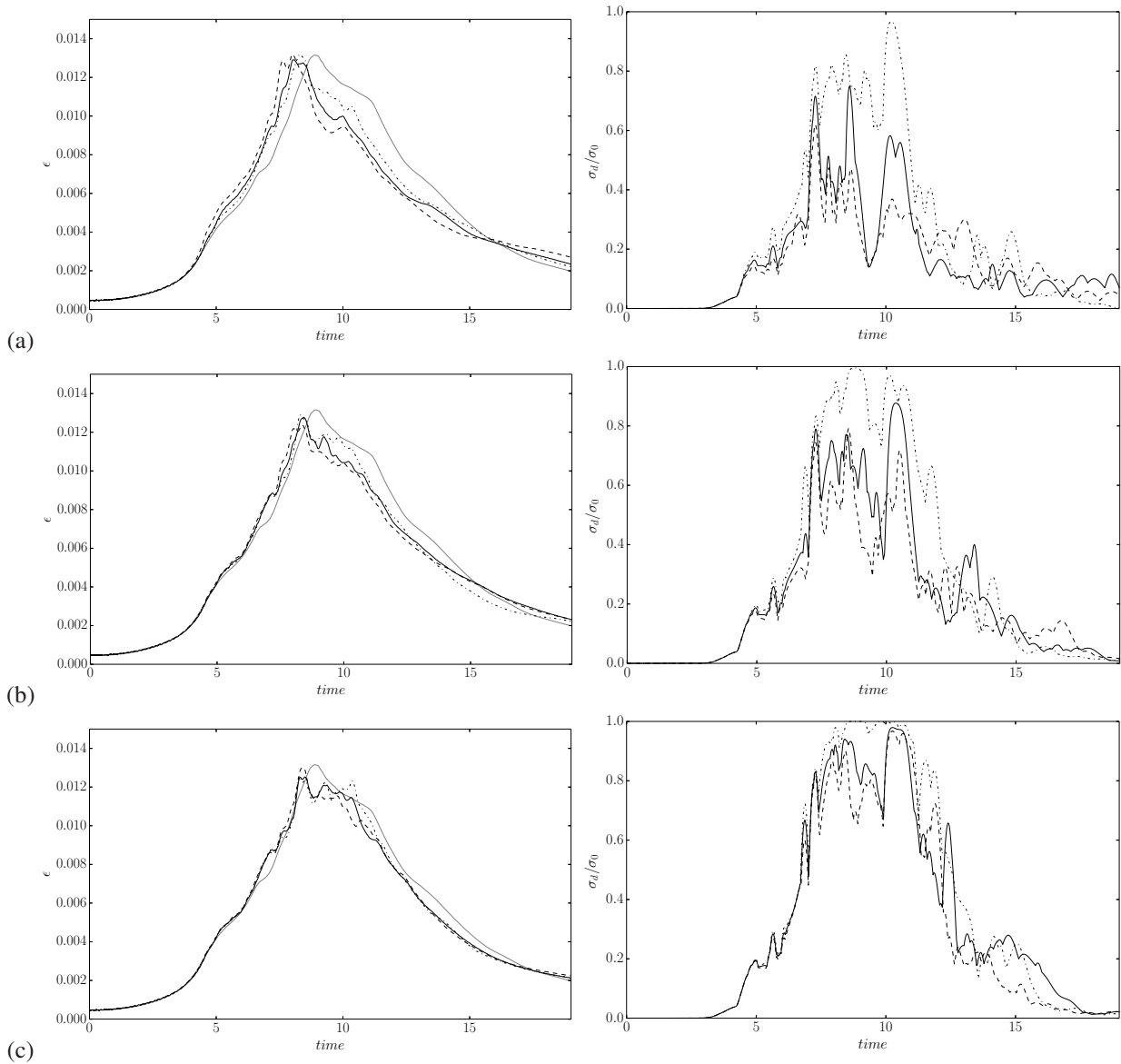
Figure 9: Influence of the σ_0 parameter. Left: Non dimensional time evolution of the dissipation rate. Right: Time trace of the maximum value of the normalized coefficient $\max[\sigma_d(\mathbf{x})]/\sigma_0$. (a): 3-point, (b) 5-point and (c)9-point filters. (— Reference simulation on 256^3) ($-\cdot-$ $\sigma_0 = 0.01$), (— $\sigma_0 = 0.05$) and (- - $\sigma_0 = 0.1$)

sensitivity. These considerations can be recast in the turbulence framework where large-scale structures are known to be more energetic. The global dissipation of the present adaptive filtering can be described by equation (9) with a coefficient $\sigma(\mathbf{k})$ dependent of the wavenumber. Indeed, the shear stress amount is expected to be higher for large and energetic structures in a turbulent flow such as Taylor-Green vortex. Then the coefficient $\sigma(\mathbf{k})$ acts as a selectivity enhancement through the term $\sigma(\mathbf{k})\mathcal{F}(\mathbf{k})$. For the present study, the frequency repartition of $\sigma(\mathbf{k})$ is imposed by the flow through S_{ij} but it is possible to design specific $\sigma(\mathbf{k})$ for LES purposes.

These tests have also emphasized the important role played by the couple (σ_0, ξ) on the simulation of a 3D decaying Taylor-Green vortex. In the following simulations, this couple will be set to $(0.05, 1.)$.
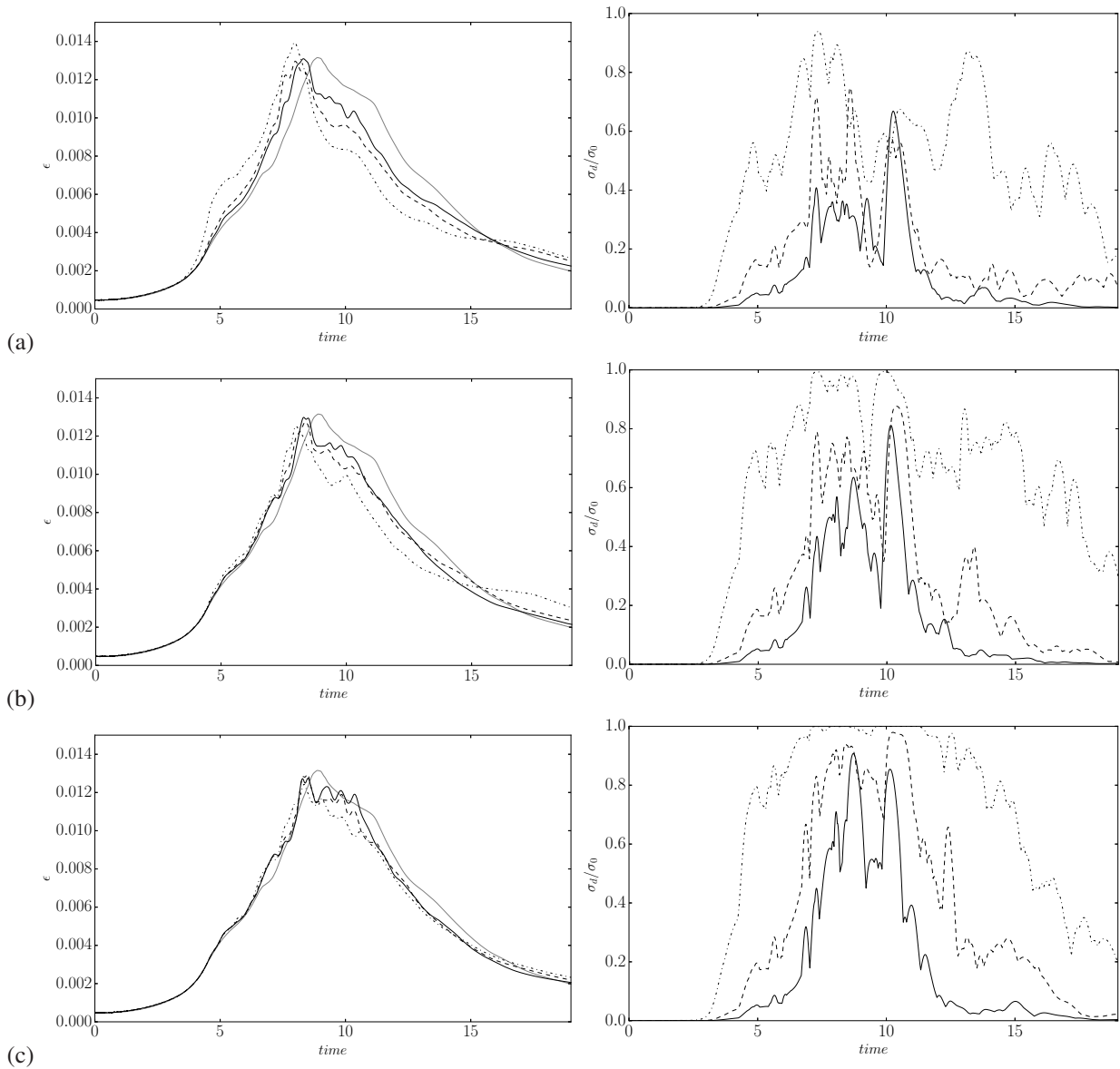
Figure 10: Influence of the parameter ξ. Left: Non dimensional time evolution of the dissipation rate. Right: Time trace of the maximum value of the normalized coefficient $\max[\sigma_d(\mathbf{x})]/\sigma_0$. (a): 3-point, (b) 5-point and (c)9-point filters. (— Reference simulation on 256^3) ($-\cdot-\xi = 0.5$), (- - $\xi = 1.0$) and (— $\xi = 1.5$)

Influence of the filtered quantity

As discussed in section 3, the filtering procedure can be applied to three different quantities which are basically the distribution functions g_α, the whole collision operator $-\frac{1}{\tau_g}(g_\alpha - g_\alpha^{eq})$ or the first moments ρ and $\rho\mathbf{u}$. The filtering of the g_α quantities is done after the propagation step, the filtering of the collision operator is done between the collision and the propagation steps and the filtering of the macroscopic quantities is done after their computations.

Figure 11 compares the influence of the filtered quantity on the dissipation of the kinetic energy for the present test-case. The observed differences indicate a weak dependence on the filter order and the better results are obtained for the filtered moments. Moreover, this latter choice induces a lower cost because only four quantities are filtered in three-dimensional simulations whereas the two other choices require the filtering of nineteen quantities. Therefore,
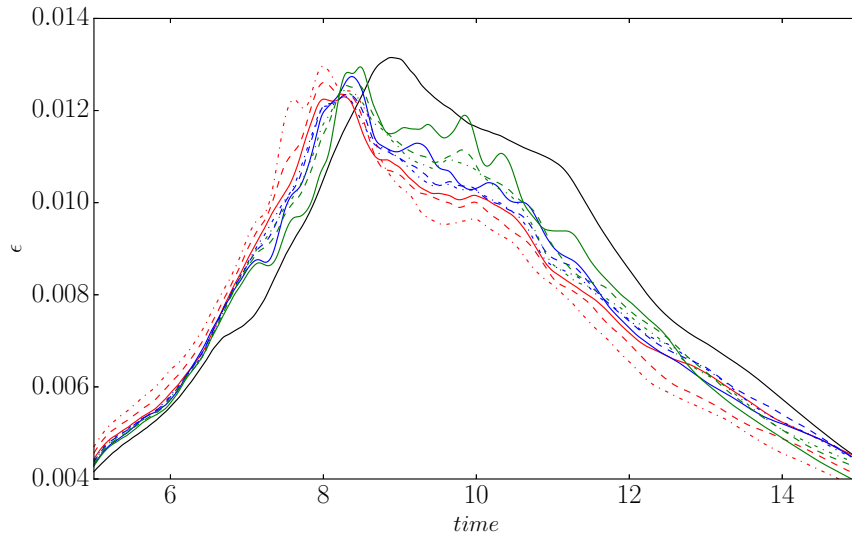
Figure 11: Comparison of the filtered quantity on a 96^3 domain with $\sigma_0 = 0.05$ and $\xi = 1.0$:(— Reference simulation on 256^3. Red, blue and green curves refers to 3-point, 5-point and 9-point filters respectively.) $-\cdot-$ filtered collision operator, $--$ filtered distribution functions, — filtered moments.

the following computations will be performed with filtered moments.

Comparison with static filters

The static filtering technique could be seen as a particular case of the dynamical one when the sensitivity is set to zero ($S_0 = 0$). Therefore, static filters act everywhere with the same amount, with potential damping of important structures in the dynamical evolution. With the above discussion, the static filtering technique is thus expected to give over-dissipated results. This is confirmed by looking at figure 12 which displays the comparison of static and dynamical filtering on a 96^3 grid (left) and a 128^3 grid (right).
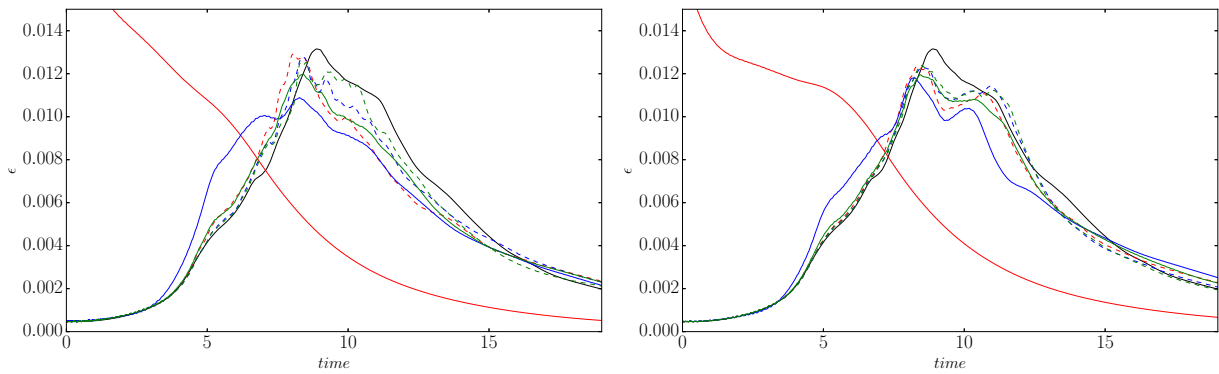

Figure 12: Comparison between static filters (solid lines) and dynamical filters (dashed lines) on a 96^3 domain (left) and a 128^3 domain (right). Red, blue and green curves refers to 3-point, 5-point and 9-point filters respectively.

A striking result is observed for 3-point stencil filter which gives completely wrong behaviour with a static strategy whereas results close to higher order filters are observed for the dynamical strategy. This is particularly apparent in the transition region where the 3-point dynamical filter gives better results than the static 5-point filter and similar results as the static 9-point filter. Moreover, the dynamical filtering appears to better predict the dissipation peak

around $t = 9$ than the static filters. The above discussions thus indicate that the results can be severely improved by increasing the filtering sensitivity and decreasing the σ_0. This behaviour suggests that the wavenumber selectivity of the spatial filters plays a minor role compared to the shear stress selectivity. Indeed, the results indicate that applying a high-order wavenumber selectivity on non-sheared quantities (*i.e.* with static filters) could lead to an over-dissipation in the transition region. As a counterpart, by introducing a shear-stress dependency on the filters, the wavenumber selectivity is forced to act on turbulent quantities with an important shear amount which corresponds to large-scale structures on which the wavenumber selectivity has no impact and could be reduced by decreasing the filter order. This result is of major importance in the framework of lattice Boltzmann method showing that relevant results could be obtained with a 3-point stencil selective filter which correspond to the LBM stencil, then conserving the locality of the scheme which is important when dealing with highly parallel implementations (see section 7).

Comparison with SGS models

The LBM implementation of subgrid-scale model is very close to the one of the present dynamical filtering. Relation (12) is used to estimate the eddy viscosity and thus the relaxation time τ_g. The comparison between the implementation of the classical Smagorinsky model and the present methodology is presented in figure 13 with the Smagorinsky model associated to a constant $C_s = 0.1$ and $C_s = 0.18$. The results indicate that the SGS implementation appears to be too dissipative and describes poorly the laminar-turbulent transition region. Similar observations are detailed in Aubard et al. [26] where various SGS strategies have been compared and found to be not suitable for this transition test case.
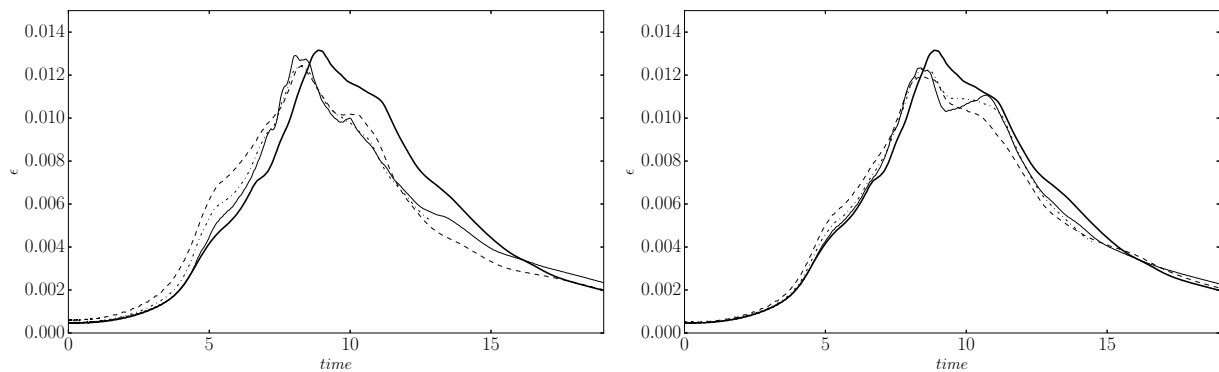

Figure 13: Comparison between dynamical filtering strategy and subgrid-scale model on a 96^3 domain (left) and a 128^3 domain (right). — reference simulation, — present filtering with 3-point filter, −− SGS with $C_s = 0.18$, −·− SGS with $C_s = 0.1$.

The present dynamical strategy is found to better predict the transition region by filtering only the sheared region. The main difference between the present implementation and the SGS methodology relies in the amount of filtering when shear stress is lower than the imposed sensitivity ($S < S_0$). Indeed for those values the filter have no impact and let the turbulent structures free of numerical dissipation. Contrariwise, the SGS implementation is directly proportional to the amount of shear stress and the eddy viscosity has a non zero value for shear stress amount close to S_0 thus imposing an over-dissipation for the corresponding structures which are of primary importance for the dynamical evolution. Moreover, the SGS approach is not a bounded procedure and the eddy viscosity can reach arbitrary high value when highly sheared region are encountered whereas the presented strategy is limited by the σ_0 value restricting the numerical dissipation to a limited amount. Finally, from a general point of view, the SGS strategy could be seen as the present dynamical filtering technique with a low shear stress sensitivity and should be linked to the results of section 6.2.2.

Computational cost

The lattice Boltzmann method is a simple, fast and local scheme which is often used for HPC simulations. Therefore computational cost issues are fundamental when introducing artifacts to the standard scheme. For the present filtering

strategy the overcost is held by the computation of relation (10) at each timestep. The comparison of the different computational cost for 2*D* and 3*D* simulations are presented in table 4. The 2D computational times refer to the test case of section 5 and the 3D computational times refer to the test-case of section 6 for a 128^3 grid. In this section, the present filtering technique is applied on the moments of the distribution functions. The present inhouse code is a set of Python modules with a time loop wrapped in Fortran-90 (f2py). All the computational time refers to a single standard processor (*Intel Xeon CPU W3565 3.20GHz*) and are given in $\mu s/point/iterations$.

Models	D2Q9		D3Q19	
Standard	0.147		0.516	
Filters	classical Filters	present Filters	classical Filters	present Filters
3-point	0.178 (+21%)	0.185 (+26%)	0.564 (+09%)	0.588 (+14%)
5-point	0.184 (+25%)	0.190 (+29%)	0.571 (+10%)	0.598 (+16%)
9-point	0.192 (+30%)	0.199 (+35%)	0.586 (+14%)	0.614 (+19%)

Table 4: Computational costs of the present filtering strategy

First, the results indicate that the overcost due to filtering is higher for 2D simulations than for 3D simulations. This can be explained by the number of discrete velocities involved in D2Q9 and D3Q19 models. For 2*D* simulations the collision and propagation steps are done on 9 velocities and the filtering of the moments are done on 3 quantities which represents 33% of the velocity number. For 3*D* simulations, the filtering is done on 4 quantities which represents 21% of the 19 velocities. Then, the overcost of the present filtering technique due to the computation of relation (10), is relatively small with an additional time of 5% in 3D compared to classical filters. This overcost must be seen in the HPC framework where communication time is of major importance. Indeed, it has been shown in the previous sections that low-stencil adaptive filter results was comparable and more stable than high stencil classical filter. These results demonstrate the ability of the present filtering technique to be used for massively parallel computations where the overcost of computing σ_d will be damped by the gain of scalability induced by low communications.

Conclusion

A dynamical filtering technique for the lattice Boltzmann method has been presented and tested on representative test-cases in 2D and 3D. It has been shown that the use of selective spatial filters with a coefficient based on the amount of shear stress led to improved stability and limited dissipation. In particular, it has been emphasized that the shear stress selectivity was restricting the action of the filters to localized zones thus reducing the global amount of numerical dissipation. The choice of shear stress selectivity has been motivated by the lattice Boltzmann framework for which the shear stress is a relevant quantity that can be accessed with a minimum amount of additional computational time. The results are particularly improved when the filter order is low, especially for the comparison with static selective filters suggesting that the wavenumber selectivity is dominated by the one of the shear stress. The comparison of the presented methodology to the classical subgrid-scale model methodology on a laminar-turbulent transition test case such as the Taylor-Green vortex have also led to promising results highlighting the importance of shear-stress selectivity in the prediction of the turbulence dynamical evolution. From a computational cost point of view, the presented strategy have shown interesting capabilities when using low-order filters thus reducing the effective stencil to the one of the LBM which is consistent with massively parallel simulations. Then the dynamical filtering strategy should be seen as an enhanced stabilization procedure for the lattice Boltzmann method where the amount of numerical dissipation is locally controlled in space. The next step will be to introduce a σ_d coefficient optimized in wavenumber space for LES purposes.

Finally it could be noticed that the presented methodology could be applied to a wide variety of numerical problems where only local dissipation is required. Moreover, the presented procedure should be extended to different physical problems by modifying the sensitive quantity and not restrict it to the shear stress. Furthermore, the presented dynamical filtering is not restricted to the Lattice Boltzmann method and could be applied to the classical finite differences schemes.

References

[1] Y.-H. Qian, D. d'Humières, P. Lallemand, Lattice BGK models for Navier-Stokes equation., Europhys.Lett. 17 (1992) 479–484.

[2] X. He, L. Luo, A priori derivation of the lattice Boltzmann equation, Phys. Rev. E 55 (1997) R6333.

[3] X. Shan, X. Yuan, H. Chen, Kinetic theory representation of hydrodynamics: a way beyond the Navier-Stokes equation., Journal of Fluid Mechanics 550 (2006) 413–441.

[4] X. Shan, H. Chen, Lattice boltzmann model for simulating flows with multiple phases and components, Phys. Rev. E 47 (3) (1993) 1815–1819.

[5] S. Marié, D. Ricot, P. Sagaut, Comparison between Lattice Boltzmann Method and Navier-Stokes high order schemes for Computational Aeroacoustics., Journal of Computational Physics. 228 (4) (2009) 1056–1070.

[6] A. Sengissen, J. Giret, C. Coreixas, J. Boussuge, Simulations of LAGOON landing-gear noise using Lattice Boltzmann Solver, in: AIAA-paper 2015-2993, 2015.

[7] J. Sterling, S. Chen, Stability analysis of lattice Boltzmann methods, J. Comp. Phys. 123 (1996) 196–206.

[8] P. Lallemand, L. Luo, Theory of the lattice Boltzmann method: Dispersion, dissipation, isotropy, Galilean invariance and stability, Phys. Rev. E 61 (06) (2000) 1–17.

[9] P. Dellar, Bulk and shear viscosities in lattice Boltzmann equations, Phys. Rev.E 64 (031203) (2003) 1–11.

[10] C. David, P. Sagaut, Structural stability of Lattice Boltzmann schemes, Physica A 444 (2016) 1–8.

[11] D. d'Humière, I. Ginzburg, Y. Krafczyk, P. Lallemand, L. Luo, Multiple relaxation time lattice Boltzmann models in three dimensions, Phil. Trans. R. Soc. Lon. A 360 (2002) 437–451.

[12] J. Latt, B. Chopard, Lattice Boltzmann method with regularized pre-collision distribution functions, Mathematics and Computers in Simulation 72 (2) (2006) 165–168.

[13] P. Lallemand, F. Dubois, Some results on energy-conserving lattice Boltzmann models, Computers and Mathematics with Applications 65 (6) (2013) 831–844.

[14] F. Tosi, S. Ubertini, S. Succi, H. Chen, I. Karlin, Numerical stability of Entropic versus positivity-enforcing Lattice Boltzmann schemes, Mathematics and Computers in Simulation 72 (2006) 227–231.

[15] D. Ricot, S. Marié, P. Sagaut, C. Bailly, Lattice Boltzmann Method with selective viscosity filters, Journal of Computational Physics. 228 (12) (2009) 4478–4490.

[16] C. Bogey, C. Bailly, A family of low dissipative explicit schemes for flow and noise computations, J. Comput. Phys. 194 (2004) 194–214.

[17] M. Germano, U. Piomelli, P. Moin, W. Cabot, A dynamic subgrid-scale eddy viscosity model, Physics of Fluids A 3 (7) (1991) 1760–1765.

[18] E. Lévêque, F. Toschi, L. Shao, J.-P. Bertoglio, Shear-improved Smagorinsky model for large-eddy simulation of wall-bounded turbulent flows, Journal of Fluid Mechanics 570 (2007) 491–502.

[19] G. Pont, P. Cinnella, J. Robinet, P. Brenner, Development of numerical schemes for hybrid RANS/LES modelling in an industrial cfd solver., in: AIAA-paper 2013-2440, 2013.

[20] C. Speziale, Turbulence Modeling for Time-Dependent RANS and VLES: A Review, AIAA Journal 36 (2) (1998) 173–184.

[21] P. Nathen, D. Gaudlitz, N. Adams, Towards wall-adaption of turbulence models within the lattice Boltzmann framework, in: International Symposium on Turbulence and Shear Flow Phenomena (TSFP-9), 2015.

[22] Y. Dong, P. Sagaut, S. Marié, Inertial consistent subgrid model for Large Eddy Simulation based on Lattice Boltzmann Method., Physics of Fluids 20 (3) (2008) 035104.

[23] O. Malaspinas, P. Sagaut, Consistent subgrid scale modelling for lattice Boltzmann methods., J. Fluid Mech. 700 (2012) 514–542.

[24] Y. Li, R. Shock, R. Zhang, H. Chen, Numerical study of flow past an impulsively started cylinder by the Lattice-Boltzmann method, Journal of Fluid Mechanics 519 (2004) 273–300.

[25] D. Fauconnier, C. Bogey, E. Dick, On the performance of relaxation filtering for large-eddy simulation, Journal of Turbulence 14 (1) (2013) 22–49.

[26] G. Aubard, P. Stefanin Volpiani, X. Gloerfelt, J.-C. Robinet, Comparison of subgrid-scale viscosity models and selective filtering strategy for large-eddy simulations, Flow Turbulence Combustion 91 (3) (2013) 497–518.

[27] P. Skordos, Initial and Boundary Conditions for the lattice Boltzmann Method., Physical Review E 48 (6) (1993) 4823–4842.

[28] M. Brachet, D. Meiron, S. Orszag, B. Nickel, R. Morf, U. Frisch, Small-scale structure of the Taylor-Green vortex., J. Fluid Mech. 130 (1983) 411–452.

[29] I. Karlin, A. Tomboulides, C. Frouzakis, S. Ansumali, Kinetically reduced local Navier-Stokes equations: An alternative approach to hydrodynamics, Phys. Rev. E 74 (035702) (2006) 1–4.